ACS APPLIED MATERIALS & INTERFACES

Letter

www.acsami.org

Photoluminescent Evolution Induced by Structural Transformation Through Thermal Treating in the Red Narrow-Band Phosphor $K_2GeF_6:Mn^{4+}$

Ling-Ling Wei,[†] Chun Che Lin,[‡] Yi-Ying Wang,[†] Mu-Huai Fang,[‡] Huan Jiao,*[,†] and Ru-Shi Liu*[,‡,§]

[†]School of Chemistry and Chemical Engineering, Shaanxi Normal University, Xi'an 710062, Shaanxi, P.R. China

[‡]Department of Chemistry, National Taiwan University, Taipei 106, Taiwan

[§]Department of Mechanical Engineering and Graduate Institute of Manufacturing Technology, National Taipei University of Technology, Taipei 106, Taiwan

Supporting Information

ABSTRACT: This study explored optimal preparation conditions for $K_2GeF_6:Mn^{4+}$ red phosphors by using chemical coprecipitation method. The prepared hexagonal $P\bar{3}m1$ $K_2GeF_6:Mn^{4+}$ exhibited efficient red emission, high color purity, good Mn^{4+} concentration stability, and low thermal quenching. Structural evolution from hexagonal $P\bar{3}m1$ to $P6_3mc$ and then $P6_3mc$ to cubic $Fm3m$ occurred after thermal treatment at approximately 400 and 500 °C, respectively. Hexagonal $P6_3mc$ phase showed an obvious zero phonon line peak at 621 nm, whereas cubic $Fm3m$ phase showed no red emission. Yellowish $K_2GeF_6:Mn^{4+}$ with both hexagonal $P\bar{3}m1$ and $P6_3mc$ symmetries are promising commercial red phosphors for white light-emitting diodes.

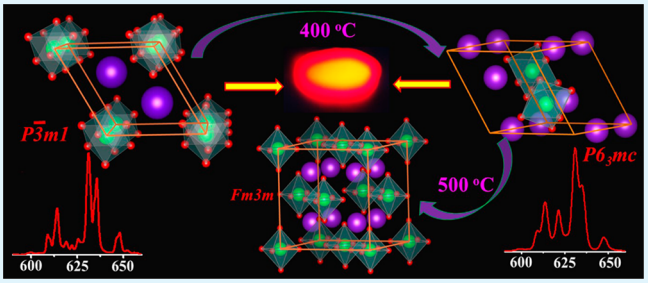

KEYWORDS: *phosphors, chemical coprecipitation method, thermal stability, structural evolution, photoluminescent properties*

Discovering new red phosphors with sufficient chemical durability and efficient luminescent properties for combining with InGaN blue diode chip and $YAG:Ce^{3+}$ yellow phosphors is important to fabricate warm white light-emitting diodes (WLEDs) with high color-rendering index (CRI, R_a > 80).[1−4] Recent studies have shown that Mn^{4+}-activated fluoride phosphors in the form of $A_2XF_6:Mn^{4+}$ (A = K, Na, Cs, NH_4; X = Si, Ge, Zr, Ti) and $BSiF_6:Mn^{4+}$ (B = Ba, Zn) can exhibit efficient red emission in 600−680 nm region.[5−13] To overcome the drawbacks of wet-chemical etching method[5−10] and hydrothermal reaction method[11−13] (such as high cost of metal wafers, time ineffectiveness of etching, dangerous factors of HF evaporation at high temperatures, and low luminescence efficiency caused by difficulty in controlling the valence state of Mn during synthesis), a simple and convenient method based on cation exchange reaction and coprecipitation has recently been proposed to synthesize $K_2TiF_6:Mn^{4+}$ and $Na_2SiF_6:Mn^{4+}$, respectivley.[14,15]

Considering that GeO_2 is more easily dissolved in HF than TiO_2 and SiO_2, we applied two-step chemical coprecipitation method in this study to synthesize $K_2GeF_6:Mn^{4+}$ red phosphors with high purity and good crystallinity without significant defects by initially synthesizing K_2MnF_6 and then precipitating $K_2GeF_6:Mn^{4+}$. The effects of reaction temperature and Mn^{4+} concentration on the phase structure and optical properties of $K_2GeF_6:Mn^{4+}$ red phosphors were studied in detail to determine the optimal preparation conditions. Additionally, in contrast to the inner 4f → 4f forbidden transition of Eu^{3+}, the outer 3d → 3d transition of Mn^{4+} (electronic configuration, $3d^3$) is sensitive to local crystal field environments in the host and can be tuned by various substitutions. Studies on Mn^{4+}-activated fluoride phosphors found that the emission shape greatly depended on the crystal structure of the host. Emission shape has two types: (1) Mn^{4+} in the host with low crystal symmetry, such as $P321$, shows an obvious zero phonon line (ZPL) peak near 620 nm; (2) Mn^{4+} in the host with crystal structures of $Fm3m$ and $P\bar{3}m1$ shows almost no ZPL peak.[8−10] In this study, the obtained $K_2GeF_6:Mn^{4+}$ with hexagonal $P\bar{3}m1$ symmetry did not show obvious ZPL peak in the emission spectra. Through thermal treating, some unique photoluminescent (PL) properties associated with structural evolution of $P\bar{3}m1$ $K_2GeF_6:Mn^{4+}$ were explored and discussed. The unique structural evolution resulted in a hexagonal $P6_3mc$ $K_2GeF_6:Mn^{4+}$ phase (showing obvious ZPL peak at 621 nm) and another cubic $Fm3m$ $K_2GeF_6:Mn^{4+}$ phase (nearly no red emission). No such special PL properties have been reported currently in any Mn^{4+}-activated fluoride phosphors.

The X-ray Rietveld refinement results and the crystal structure of $K_2GeF_6:Mn^{4+}$ synthesized at 20 °C are shown in Figure 1a. The X-ray Rietveld refinement results of

Received: March 14, 2015
Accepted: May 11, 2015
Published: May 11, 2015

DOI: 10.1021/acsami.5b02212
ACS Appl. Mater. Interfaces 2015, 7, 10656−10659

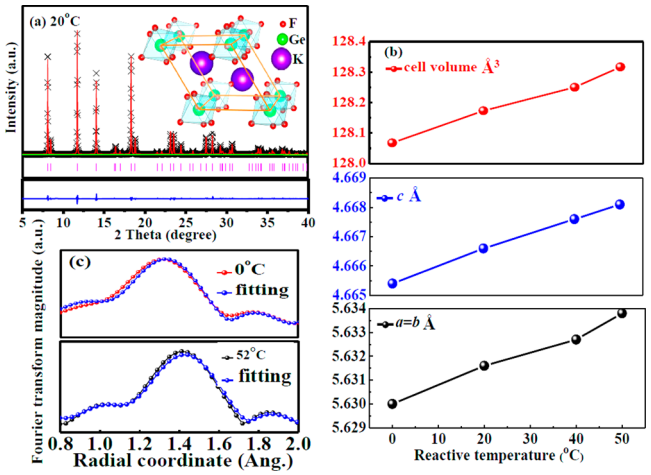

Figure 1. Structural results of $K_2GeF_6:Mn^{4+}$ phosphors. (a) X-ray Rietveld refinements of $K_2GeF_6:Mn^{4+}$ synthesized at 20 °C. (b) Variations in cell parameters with reactive temperature. (c) Fourier-transform-fitted EXAFS spectra for $K_2GeF_6:Mn^{4+}$ synthesized at 0 and 52 °C, respectively.

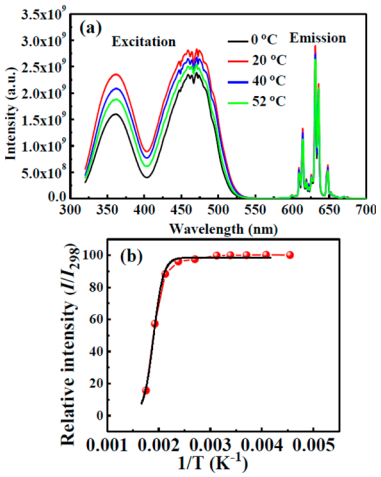

Figure 2. (a) Experimental excitation and emission spectra of $K_2GeF_6:Mn^{4+}$. (b) Temperature dependence of integrated PL intensity relative to 298 K for $K_2GeF_6:Mn^{4+}$.

$K_2GeF_6:Mn^{4+}$ synthesized at 0, 40, and 52 °C are shown in Figure S1 in the Supporting Information. All samples show similar XRD patterns indexed to the hexagonal $P\bar{3}m1$ symmetry (JCPDS No. 73−1531). No traces of residual K_2MnF_6 and other impurities can be observed. Figure 1b shows the shifts of crystallographic parameters from X-ray Rietveld refinements with reactive temperature for $K_2GeF_6:Mn^{4+}$. The crystallographic parameters a (b) and c linearly increase with reactive temperature, resulting in slight expansion of the crystal volume. Figure 1c suggests that the two samples synthesized at 0 and 52 °C exhibit same coordination environments of Ge^{4+}. Meanwhile, the bond length between Ge^{4+} and ligand F^- ions for the sample synthesized at 52 °C (1.810 Å) is longer than that of the sample synthesized at 0 °C (1.776 Å), further verifying the slight crystal expansion with increasing reactive temperature. Figure S2 in the Supporting Information exhibits the microstructures of $K_2GeF_6:Mn^{4+}$ phosphors synthesized at different temperatures by scanning electron microscopy (SEM). SEM images indicate that all $K_2GeF_6:Mn^{4+}$ powders have hexagonal shape with particle size in the range of 20−100 μm. The particle size gradually increases with increasing reactive temperature, and the phosphors synthesized at 20 °C in Figure S2b in the Supporting Information show a uniform size.

Figure 2a illustrates the excitation and emission spectra of $K_2GeF_6:Mn^{4+}$ synthesized at different temperatures. Consistent with the reported results on other Mn^{4+}-activated fluoride compounds, two broad excitation bands appear in the range of 320−500 nm, corresponding to the spin-allowed transitions of $^4A_2 \rightarrow {}^4T_1$ and $^4A_2 \rightarrow {}^4T_2$, respectively.[5−10] The sharp red emission lines in the range of 600−650 nm originate from the spin-forbidden $^2E \rightarrow {}^4A_2$ transition. Considering Figure S2 in the Supporting Information, $K_2GeF_6:Mn^{4+}$ red phosphors synthesized at 20 °C with uniform size show the most efficient emission intensity. Influences of Mn^{4+} concentration on the phase purity and optical properties of $K_2Ge_{1-x}Mn_xF_6$ are shown in Figures S3 and S4 in the Supporting Information. Only the sample with x = 0.084 shows weak characteristic XRD patterns of residual K_2MnF_6. The integrated PL intensity for phosphors with x = 0.057, 0.063, 0.070 changes slightly, suggesting that $K_2Ge_{1-x}Mn_xF_6$ phosphors show stable and effective red emission, which is beneficial to industrial production. Figure 2b shows considerable thermal stability for $K_2GeF_6:Mn^{4+}$ red phosphors in the temperature range of 298−573 K. The relative integrated PL intensity I_{PL}/I_{PL298} at 423 K is above 95%, which is higher than that of rare-earth doped nitride red phosphors. The activation energy obtained for $K_2GeF_6:Mn^{4+}$ red phosphors is 0.93 eV, nearly four times higher than that (0.23 eV) of nitride compounds. The prepared $K_2GeF_6:Mn^{4+}$ powders exhibit efficient red emission, high color purity, good Mn^{4+} concentration stability, and low thermal quenching; thus, these substances can be used in commercial applications.

The following section mainly discusses the unique PL and structural evolution under thermal treating for $K_2GeF_6:Mn^{4+}$ synthesized at optimal conditions. Figure 3a shows that with

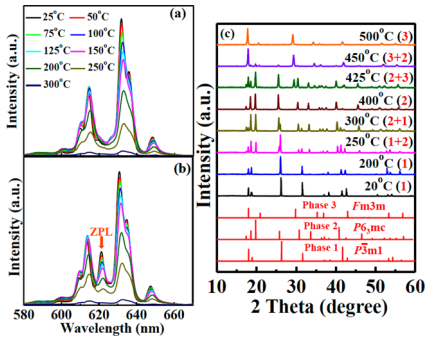

Figure 3. Photoluminescent and structural evolution of $K_2GeF_6:Mn^{4+}$ phosphors. (a) Dependence of PL spectra with temperature during heating cycle. (b) Dependence of PL spectra with temperature during cooling cycle. (c): XRD patterns of $K_2GeF_6:Mn^{4+}$ during thermal treating.

increasing temperature from 25 to 300 °C, all emission lines become broader and red-shift because of the increased absorbed phonons and enhanced vibration transition coupling associated with the vibration modes of the MnF_6^{2-} octahedron. Meanwhile, the PL intensity decreases because of thermal quenching, leading to very weak red emission when the measuring temperature is 300 °C. After further decreasing the measuring temperature from 300 to 25 °C during cooling cycle (Figure 3b), the main emission peaks at ~609, 613, 631, 635,

DOI: 10.1021/acsami.5b02212
ACS Appl. Mater. Interfaces 2015, 7, 10656−10659

and 648 nm (associated with anti-Strokes ν_4, ν_6 and Strokes ν_6, ν_4, ν_3) are similar to those in Figure 3a. Interestingly, an obvious ZPL peak is also observed at 621 nm (1.997 eV), and its intensity gradually increases with decreasing temperature. To further clarify the above behavior, the simultaneous temperature dependence of XRD measurement was performed on K_2GeF_6:Mn^{4+} and shown in Figure 3c. No structural change occurs and only pure $P\bar{3}m1$ (phase 1) is observed below 200 °C. With increasing temperature to 250 °C, $P6_3mc$ (phase 2) emerges, whereas the main phase is still $P\bar{3}m1$. Pure $P6_3mc$ phase is obtained at 400 °C. Sequentially, another cubic $Fm3m$ (phase 3) is obtained when temperature is higher than 425 °C. For Mn^{4+}-activated fluoride phosphors, obvious ZPL peak exists only in the host structure with low symmetry, such as the D_3-$P321$ and D_{2h}-F_{ddd} symmetries.[7,9] Then it is reasonable in Figure 3a that the K_2GeF_6:Mn^{4+} heated at 250 °C with main $P\bar{3}m1$ phase shows no ZPL emission, whereas the $P6_3mc$ phase obtained after measuring PL properties at 300 °C shows an obvious ZPL peak.

Figure 4a shows the structural evolution schematic during heat treatment of K_2GeF_6. The three symmetries have similar

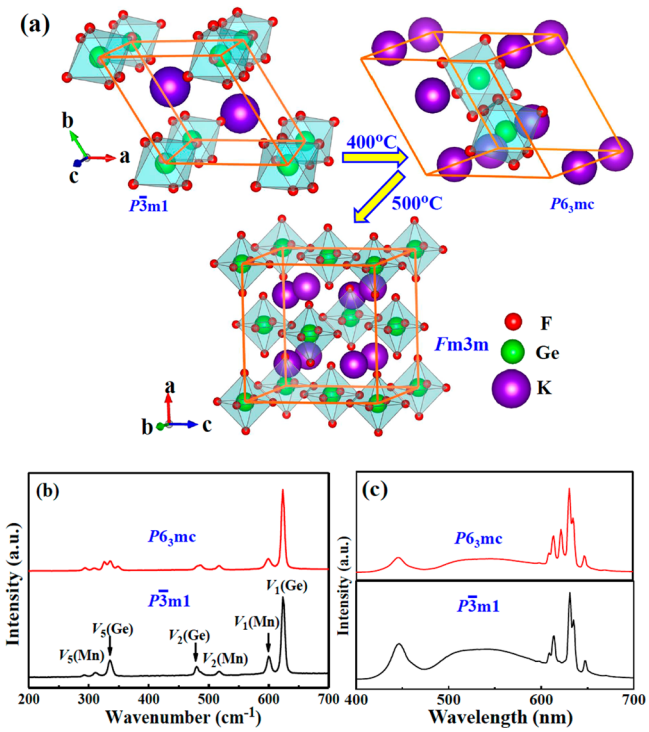

Figure 4. (a) Schematic of structural evolution during heat treatment of K_2GeF_6. (b) Raman scattering spectra of K_2GeF_6:Mn^{4+} before and after heat treatment. (c) Luminescence spectra of the WLEDs using K_2GeF_6:Mn^{4+} red phosphors.

coordination environments of MnF_6^{2-} octahedron, but the crystal structure differs with each other significantly. Mn^{4+} ions in $Fm3m$ K_2GeF_6 host show O_h symmetry, whereas the site symmetries of Mn^{4+} ions in $P\bar{3}m1$ and $P6_3mc$ hosts reduce to D_{3d} and C_{6v}, respectively. O_h have six fundamental internal vibronic modes: $\nu_1(A_{1g})$, $\nu_2(E_g)$, $\nu_3(T_{1u})$, $\nu_4(T_{1u})$, $\nu_5(T_{2g})$, and $\nu_6(T_{2u})$. In D_{3d} symmetry, the triply degenerate modes ν_3, ν_4, ν_5, and ν_6 further split into a doubly degenerate and a nondegenerate modes because of octahedral distortion.[8,15] The antisymmetric vibronic modes coupled to the ZPLs of $^2E \rightarrow {}^4A_2$ results in the splitting phenomenon for emission lines, and leads to the broader emission spectra of K_2GeF_6:Mn^{4+}compared with sharp emission lines of K_2SiF_6:Mn^{4+} (Figure S5 in the Supporting Information). The split energies of ν_3, ν_4, ν_5, and ν_6 enhances in lower C_{6v} symmetry. This can be verified by the fact that $P6_3mc$ K_2GeF_6:Mn^{4+} calcined at 400 °C for 20 min in air shows obvious split behavior for ν_5 vibration mode at ~330 cm^{-1} according to Figure 4b. Figure S6 in the Supporting Information shows that the yellowish K_2GeF_6:Mn^{4+} powders with both $P\bar{3}m1$ and $P6_3mc$ symmetries yield bright red emission upon excitation of 460 nm blue light, whereas light purple cubic K_2GeF_6:Mn powders show nearly no red emission which may be due to the reduction of Mn valence from 4+ to 2+ as evidence by the X-ray absorption near-edge structure using synchrotron radiation (Figure S7 in the Supporting Information). Luminescent spectra of the WLEDs (fabricated with blue InGaN chips, $Y_3Al_5O_{12}$:Ce^{3+} yellow phosphor, and K_2GeF_6:Mn^{4+} red phosphors) shown in Figure 4c reconfirm the obvious ZPL peak for $P6_3mc$ symmetry. The color temperatures of 3974 and 3363 K are determined for WLEDs that comprise red K_2GeF_6:Mn^{4+} phosphors with $P\bar{3}m1$ and $P6_3mc$ symmetries, respectively. CRI values of 86 and 89 are obtained under a drive current of 15 mA for both symmetries. These results indicate that the two K_2GeF_6:Mn^{4+} red phosphors show great promise for commercial applications.

In summary, the optimal preparation conditions were explored for K_2GeF_6:Mn^{4+} red phosphors by using chemical coprecipitation. This study confirmed K_2GeF_6:Mn^{4+} as a promising red phosphor candidate based on the following advantages: synthesis temperature of 20 °C, quick dissolution of GeO_2 in HF, and optimal photoluminescent properties. The unique PL properties associated with structural evolution of K_2GeF_6:Mn^{4+} was also studied. The new hexagonal $P6_3mc$ K_2GeF_6:Mn^{4+} phase showed obvious ZPL peak at 621 nm, whereas another cubic $Fm3m$ K_2GeF_6:Mn^{4+} phase showed nearly no red emission.

■ ASSOCIATED CONTENT

Supporting Information

This section includes the experimental details, theoretical calculations, supporting tables and figures of the additional crystallography data, SEM images, and photoluminescent properties.The Supporting Information is available free of charge on the ACS Publications website at DOI: 10.1021/acsami.5b02212.

■ AUTHOR INFORMATION

Corresponding Authors

*E-mail: jiaohuan@snnu.edu.cn.
*E-mail: rsliu@ntu.edu.tw.

Notes

The authors declare no competing financial interest.

■ ACKNOWLEDGMENTS

The authors thank the Industrial Technology Research Institute (Contract D351A41300) and Ministry of Science and Technology of Taiwan (Contract MOST 101-2113-M-002-014-MY3) for financially supporting this work. H.J. is grateful for financial support by the National Natural Science Foundation of China (No. 51272151) and the Fundamental Research Fund for the Central Universities (GK201402052, and GK201305013). Lingling Wei is grateful for financial

DOI: 10.1021/acsami.5b02212
ACS Appl. Mater. Interfaces 2015, 7, 10656−10659

support by the National Natural Science Foundation of China (21401123), the Fundamental Research Fund for the Central Universities (GK201402061), and the China Postdoctoral Science Foundation funded project (2014M562367).

REFERENCES

(1) Huang, C. H.; Chen, T. M. Novel Yellow-Emitting $Sr_8MgLn(PO_4)_7:Eu^{2+}$ (Ln = Y, La) Phosphors for Applications in White LEDs with Excellent Color Rendering Index. *Inorg. Chem.* **2011**, *50*, 5725−5730.

(2) Roushan, M.; Zhang, X.; Li, J. Solution-Processable White-Light-Emitting Hybrid Semiconductor Bulk Materials with High Photoluminescence Quantum Efficiency. *Angew. Chem., Int. Ed.* **2012**, *124*, 451−454.

(3) Li, H. F.; Zhao, R.; Jia, Y. L.; Sun, W. Z.; Fu, J. P.; Jiang, L. H.; Zhang, S.; Pang, R.; Li, C. Y. $Sr_{1.7}Zn_{0.3}CeO_4:Eu^{3+}$ Novel Red-Emitting Phosphors: Synthesis and Photoluminescence Properties. *ACS Appl. Mater. Interfaces* **2014**, *6*, 3163−3169.

(4) Pust, P.; Weiler, V.; Hecht, C.; Tucks, A.; Wochnik, A. S.; Hen, A. K.; Wiechert, D.; Scheu, C.; Schmid, P. J.; Schnick, W. Narrow-Band Red-Emitting $Sr(LiAl_3N_4):Eu^{2+}$ as a Next-Generation LED-Phosphor Material. *Nat. Mater.* **2014**, *13*, 891−896.

(5) Takahashi, T.; Adachi, S. Mn^{4+}-Activated Red Photoluminescence in K_2SiF_6 Phosphor. *J. Electrochem. Soc.* **2008**, *155*, E183−E188.

(6) Adachi, S.; Takahashi, T. Photoluminescent Properties of $K_2GeF_6:Mn^{4+}$ Red Phosphor Synthesized from Aqueous HF/$KMnO_4$ Solution. *J. Appl. Phys.* **2009**, *106*, 013516−1−6.

(7) Xu, Y. K.; Adachi, S. Properties of $Na_2SiF_6:Mn^{4+}$ and $Na_2GeF_6:Mn^{4+}$ Red Phosphors Synthesized by Wet Chemical Etching. *J. Appl. Phys.* **2009**, *106*, 013525−1−6.

(8) Xu, Y. K.; Adachi, S. Properties of Mn^{4+}-Activated Hexafluorotitanate Phosphors. *J. Electrochem. Soc.* **2011**, *158*, J58−J65.

(9) Arai, Y.; Adachi, S. Photoluminescent Properties of $K_2SnF_6\cdot H_2O:Mn^{4+}$. *J. Electrochem. Soc.* **2011**, *158*, J81−J85.

(10) Kasa, R.; Adachi, S. Red and Deep Red Emissions from Cubic $K_2SiF_6:Mn^{4+}$ and Hexagonal K_2MnF_6 Synthesized in HF/$KMnO_4$/KHF_2/Si Solutions. *J. Electrochem. Soc.* **2012**, *159*, J89−J95.

(11) Jiang, X. Y.; Pan, Y. X.; Huang, S. M.; Chen, X. A.; Wang, J. G.; Liu, G. K. Hydrothermal Synthesis and Photoluminescence Properties of Red Phosphor $BaSiF_6:Mn^{4+}$ for LED Applications. *J. Mater. Chem. C* **2014**, *2*, 2301−2306.

(12) Lv, L. F.; Jiang, X. Y.; Huang, S. M.; Chen, X. A.; Pan, Y. X. The Formation Mechanism, Improved Photoluminescence and LED Applications of Red Phosphor $K_2SiF_6:Mn^{4+}$. *J. Mater. Chem. C* **2014**, *2*, 3879−3884.

(13) Jiang, X. Y.; Chen, Z.; Huang, S. M.; Wang, J. G.; Pan, Y. X. A Red Phosphor $BaTiF_6:Mn^{4+}$: Reaction Mechanism, Microstructures, Optical Properties, and Applications for White LEDs. *Dalton Trans.* **2014**, *43*, 9414−9417.

(14) Zhu, H. M.; Lin, C. C.; Luo, W. Q.; Shu, S. T.; Liu, Z. G.; Wang, M.; Kong, J. T.; Ma, E.; Cao, Y. G.; Liu, R. S.; Chen, X. Y. Highly Efficient Non-Rare-Earth Red Emitting Phosphor for Warm White Light-Emitting Diodes. *Nat. Commun.* **2014**, *5*, 4312−1−10.

(15) Nguyen, H. D.; Lin, C. C.; Fang, M. H.; Liu, R. S. Synthesis of $Na_2SiF_6:Mn^{4+}$ Red Phosphors for White LED Applications by Co-Precipitation. *J. Mater. Chem. C* **2014**, *2*, 10268.

DOI: 10.1021/acsami.5b02212
ACS Appl. Mater. Interfaces 2015, 7, 10656−10659